Engineering 18 (2022) 207–217

Contents lists available at ScienceDirect

Engineering

journal homepage: www.elsevier.com/locate/eng

Research
Hydraulic Engineering—Article

Xin'anjiang Nested Experimental Watershed (XAJ-NEW) for Understanding Multiscale Water Cycle: Scientific Objectives and Experimental Design

Ke Zhang [a,b,c], Yunping Li [a,b], Zhongbo Yu [a,b,c,*], Tao Yang [a,b,c], Junzeng Xu [a], Lijun Chao [a], Jin Ni [d], Liutong Wang [d], Yun Gao [a], Yuzhong Hu [e], Zuoding Lin [f]

[a] State Key Laboratory of Hydrology-Water Resources and Hydraulic Engineering, Hohai University, Nanjing 210098, China
[b] Yangtze Institute for Conservation and Development, Hohai University, Nanjing 210098, China
[c] College of Hydrology and Water Resources, Hohai University, Nanjing, 210098, China
[d] Bureau of Hydrology (Information Center) of Taihu Basin Authority, Shanghai 200434, China
[e] Bureau of Hydrology of Anhui Province, Hefei 230022, China
[f] Department of Hydrology, Chinese Ministry of Water Resources, Beijing 100053, China

ARTICLE INFO

Article history:
Received 19 February 2021
Revised 29 July 2021
Accepted 6 August 2021
Available online 22 December 2021

Keywords:
Water cycle
Runoff generation
Hydrological processes
Hydrological scaling
Soil moisture
Groundwater
Canopy interception

ABSTRACT

This paper presents the background, scientific objectives, experimental design, and preliminary achievements of the Xin'anjiang nested experimental watershed (XAJ-NEW), implemented in 2017 in eastern China, which has a subtropical humid monsoon climate and a total area of 2674 km^2. The scientific objectives of the XAJ-NEW include building a comprehensive, multiscale, and nested hydrometeorological monitoring and experimental program, strengthening the observation of the water cycle, discovering the spatiotemporal scaling effects of hydrological processes, and revealing the mechanisms controlling runoff generation and partitioning in a typical humid, hilly area. After two years of operation, preliminary results indicated scale-dependent variability in key hydrometeorological processes and variables such as precipitation, runoff, groundwater, and soil moisture. The effects of canopy interception and runoff partitioning between the surface and subsurface were also identified. Continuous operation of this program can further reveal the mechanisms controlling runoff generation and partitioning, discover the spatiotemporal scaling effects of hydrological processes, and understand the impacts of climate change on hydrological processes. These findings provide new insights into understanding multiscale hydrological processes and their responses to meteorological forcings, improving model parameterization schemes, and enhancing weather and climate forecast skills.

1. Introduction

The water cycle, consisting of a series of hydrological processes, including atmospheric moisture transportation, precipitation, evapotranspiration, infiltration, runoff generation, and runoff concentration, is an essential component of the climate system [1,2]. Movement of water through the liquid, solid, and vapor phases is the most active process in the ecosystem involving the biological, chemical, and physical exchange of water, energy, and carbon between the land surface and the atmosphere [3,4]. Because climate dynamics, human activities, and land use/land cover changes on multiple spatiotemporal scales influence the complex water cycle processes [3,5–7], understanding and quantifying the complex hydrological processes in a changing environment has become a major scientific endeavor [4,8,9].

Experiments on and observation of water cycle elements are the foundation to understanding various hydrological processes. However, a lack of reliable data is a longstanding challenge to quantitatively understanding the global water and energy exchange [10,11]. Many experiments have been conducted to understand the local, regional, and global water and energy cycles in recent decades, such as the Global Energy and Water Cycle Experiment in the 1990s [11,12] and the Coordinated Enhanced Observing Period launched in 2001 [13]. The United States Department of

* Corresponding author.
E-mail address: zyu@hhu.edu.cn (Z. Yu).

https://doi.org/10.1016/j.eng.2021.08.026

Agriculture established the well-known Walnut Gulch Experimental Watershed in 1953 to study soil erosion and land degradation problems. It gradually evolved into a comprehensive experimental watershed with multiple functionalities for understanding hydrology and ecosystems and interactions between water supply and water quality in a typical semi-arid region [14–17]. Hydrological experiments have played a critical role in discovering hydrological mechanisms, advancing the hydrology discipline, and developing and verifying new and existing theories and models [16,18–21]. The experimental studies of hillslope hydrology under different conditions worldwide [22–26] have boosted the development of hillslope hydrology and provided a basis for discovering important hydrological theories such as the runoff generation mechanisms under saturated storage and variable contributing area, assuming that only partial catchment areas with saturated storage contribute to runoff [27–30]. It further catalyzed the development of hydrological models, such as the Hydrologiska Byråns Vattenbalansavdelning model [31,32], topography based hydrological model [33], Xin'anjiang model [27], variable infiltration capacity model [34], hydrologic model system (HMS) [2,8], and grid-topography-based distributed hydrological model [35]. More recently, with the availability of new data and techniques, significant progress has been made on identifying and representing the spatial heterogeneity of runoff generation based on topography- and physics-based estimation of root zone storage [36–38] and topography and land cover/land use [39].

In recent years, China has launched several field camps and regional observation programs in its northwestern semi-arid and arid regions and the Tibetan Plateau, including the Heihe Watershed Allied Telemetry Experimental Research, launched in 2012 to improve the observability of hydrological and ecological processes in the Heihe Watershed of northwestern China [40], multiscale soil moisture and freeze–thaw monitoring network in the Tibetan Plateau established in 2012 [41], and third atmospheric scientific experiment over the Tibetan Plateau to build integrated monitoring systems for the land surface, boundary layer, troposphere, and lower stratosphere [42]. These studies have provided valuable first-hand ground truths to validate model simulations and assess climate change impacts. Ground and satellite observations show that climate change has intensified the water cycle and altered the spatiotemporal distribution of water over large regions [9,43–45]. Because detailed information on fine-scale and multiscale hydrological processes is limited, further studies on the first-order hydrological processes and diurnal–seasonal-inter annual variations of various hydrological processes and mechanisms controlling the water cycle in the changing environment on fine and multiple scales [46,47] are required for more accurate future projections.

Hydrological data are the basis for an accurate understanding of the water cycle. Hydrological variables, such as rainfall, evaporation, soil water content, groundwater level, and streamflow, are obtained through remote sensing technology and *in situ* observations. Although remote sensing techniques can provide spatially continuous *in situ* observations of hydrological variables, they cannot provide temporally continuous coverage and capture fine-scale key processes [10,48]. Furthermore, remote sensing relies on *in situ* observations for calibration and performance evaluation [10,48]. However, scaling is hampered by the combined remote sensing and *in situ* observation data [49–51]. Addressing these challenges requires developing holistic, multiscale observations for more accurate quantification [52].

Humid regions, mainly located in eastern and southeastern China, account for approximately 32% of the total area. Topography in eastern China varies greatly in space and creates large landscape heterogeneity. The Xin'anjiang model [53] was developed based on the saturation–excess runoff generation mechanism inferred from the observed hydrological data in the Xin'anjiang Watershed in the eastern China humid zone. The Xin'anjiang Watershed has frequent high-intensity rainfall and rapid response to hydrological processes, which can easily lead to flash floods. Flooding due to extremely intense rainfall is among the most severe natural disasters in eastern China [54]. Some studies have shown that eastern China has experienced an increasing trend in extreme rainfall [55–57]. According to a recent Intergovernmental Panel on Climate Change (IPCC) report 2020, eastern China is projected to suffer large climate changes and experience intense climate change-induced hydrometeorological extremes. Understanding the hydrological processes at different scales and their responses to meteorological forcing is the key to preventing flood hazards and relieving their impacts in the region [2,8]. Accurate observation in the Xin'anjiang Watershed is critical to understanding the hydrological processes, flood formation mechanisms, and water cycle under the changing environment in eastern China humid zones and other similar regions.

In this study, we present the background, scientific objectives, experimental design, and preliminary achievements of the Xin'anjiang nested experimental watershed (XAJ-NEW), established in 2017, to understand the multiscale hydrological processes in China's typical subtropical humid monsoon region.

2. Scientific objectives

The scientific objectives of the XAJ-NEW were to build a comprehensive, multiscale, and nested hydrometeorological monitoring and experimental system to strengthen the observation of the water cycle in a typical humid, hilly area of eastern China, discover the spatiotemporal scaling effects of hydrological processes through the observations of the multiscale nested watersheds, and reveal the mechanisms controlling runoff generation and partitioning and the interaction and feedback among various processes. XAJ-NEW observes key hydrometeorological variables, including rainfall, soil moisture, groundwater depth, interception, and runoff components. The observation instruments and facilities were constructed per the relevant standards and gradually implemented since August 2017.

Network observations provide key hydrometeorological variables and processes at a fine temporal scale and across multiple spatial scales in a spatially nested fashion to accurately measure hydrological processes and their spatial heterogeneities. Because hydrological processes are influenced by complex topography and meteorological conditions, observations of hydrological variables should be enhanced at both spatial and temporal scales. For example, rainfall stations are densely distributed in typical watersheds. In addition, the observations of these variables range from minutes to hours in the XAJ-NEW.

The experiments observe key hydrological processes and meteorological variables to better understand the important ecohydrological processes and underlying mechanisms. For example, the observations at the XAJ-NEW quantifies the canopy interception and runoff partitioning process through the rainfall gauging array and runoff component observing system, respectively. These important processes in hydrology are often simulated using empirical methods. The canopy rainfall interception instrument quantitatively observes the interception ratio under different rainfall intensities and canopy conditions and provides the ground truth to develop more accurate equations to simulate interception. In the Xin'anjiang model, runoff separation includes three components: surface, interflow, and subsurface runoffs [53,58–60]. The runoff component observation system directly measures the surface runoff and interflow under different soil depths, further improving our knowledge of the natural runoff partitioning

process. Moreover, the root zone is the most active soil layer for the transfer and partitioning of water and energy and plays a key link between the water cycle and vegetation dynamics [61]. An array soil moisture gauging network, implemented in the XAJ-NEW, observes soil moisture from the topsoil to 60 cm below the ground. Groundwater monitoring platforms were also installed in the XAJ-NEW to monitor the groundwater dynamics and aeration zone. In addition, the flux tower in the XAJ-NEW observes the meteorological variables at different heights and capture the exchange of water vapor, CO_2, and energy between the terrestrial ecosystem and atmosphere. These observations aid the development of accurate ecohydrological processes and improve the hydrological and land surface models.

3. Experimental area and network design

3.1. Study area

3.1.1. Tunxi Watershed

The XAJ-NEW was implemented across the entire Tunxi Watershed (Fig. 1(a)). Tunxi Watershed is the headstream of the Xin'anjiang Watershed and is located in Huangshan, Anhui Province (Fig. 1(a)), China. The region has a humid climate and a drainage area of 2674 km^2 [62–64]. The average annual rainfall and temperature were approximately 1800 $mm \cdot a^{-1}$ and 17 °C, respectively. In the XAJ-NEW, the Tunxi Watershed was divided into five-tier nested watersheds (Fig. 1) as follows: the 5th-tier Tunxi Watershed (Fig. 1(a)), 4th-tier Yuetan Watershed (Fig. 1(a)), 3rd-tier Zhonghecun Watershed (Fig. 1(a)), two 2nd-tier watersheds (2nd-tier Watershed I and 2nd-tier Watershed II) located within the Zhonghecun Watershed (Fig. 1(b)), and two 1st-tier watersheds (1st-tier Watershed I and 1st-tier Watershed II) located within the 2nd-tier Watershed II (Figs. 1(c) and (d)). Vegetation in this region is dominated by evergreen broadleaf forest, evergreen needleleaf trees, and bamboo.

3.1.2. 2nd-and 1st-tier watersheds

The two typical 2nd-tier watersheds, located in the Mukeng village, Huangshan, are part of the Zhonghecun Watershed (Fig. 1(b)). Named the Xin'anjiang Monitoring and Experimental Field Center (hereinafter referred to as typical catchments), they are adjacent with a drainage area of 0.35 km^2 (2nd-tier Watershed I on the left) and 0.23 km^2 (2nd-tier Watershed II on the right), respectively. The mean slope of the 2nd-tier watersheds is approximately 30°. The

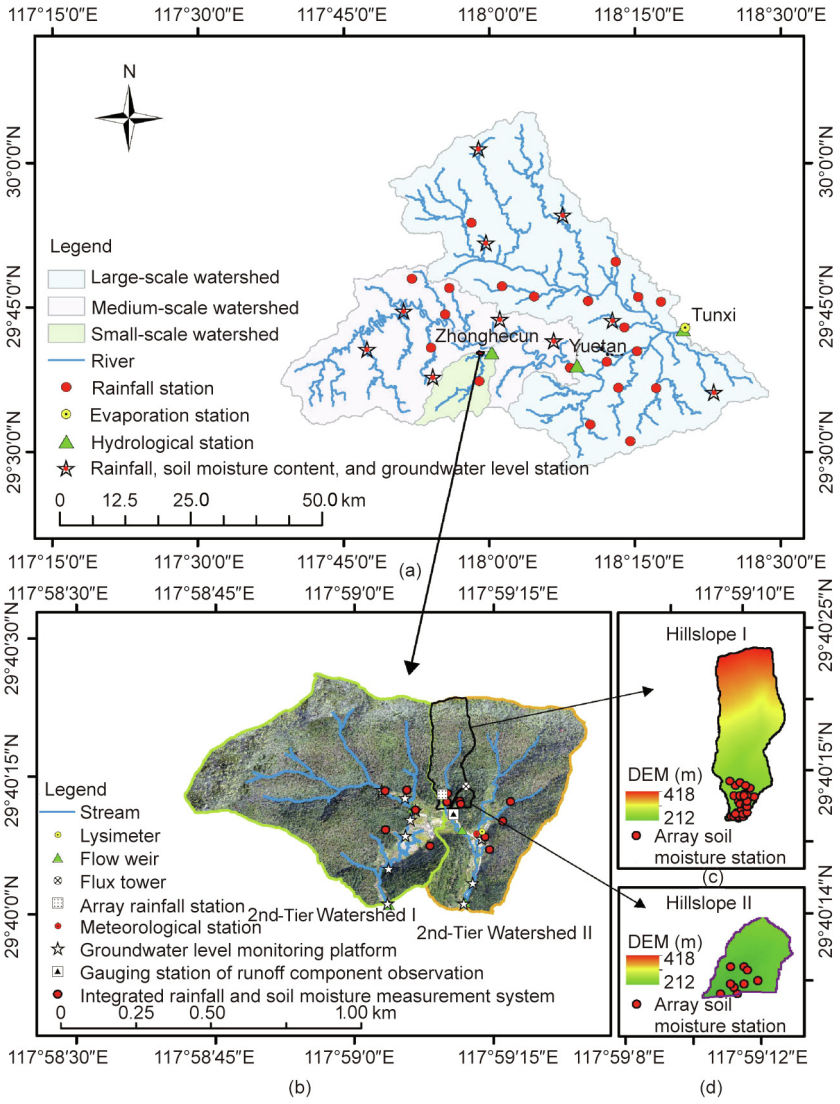

Fig. 1. Location and configuration of the XAJ-NEW: (a) geographical locations of the five-tier nested watersheds and spatial distributions of gauging stations, (b) locations of the two 2nd-tier watersheds and distributions of their gauging stations, (c) topography of 1st-tier Watershed I within the 2nd-tier Watershed II, and (d) topography of 1st-tier Watershed II within the 2nd-tier Watershed II. DEM: digital elevation model.

soil in this region is mainly sandy and clayey, and soil depth varies between 5–8 m. The two watersheds represent the topography, geomorphology, geology, and meteorology across the Tunxi Watershed. The two 1st-tier watersheds are heavily and intensely gauged to observe the hydrometeorological states to study the canopy interception, surface runoff, interflow, soil water content, and evapotranspiration.

3.2. Network configuration

The design of the XAJ-NEW is based on the idea of building a comprehensive, multiscale, and nested hydrometeorological monitoring and experimental system. It comprises five tiers of nested watersheds with areas ranging from 0.003 to 2674 km^2 (Fig. 1). Tunxi Watershed is the ultimate outlet of the XAJ-NEW (Fig. 1). The implementation of the XAJ-NEW takes advantage of existing gauging systems, including hydrological stations and rain gauges implemented by the Hydrological Bureau of Anhui Province. The layout and location selections of all hydrological gauges follow the Technical Regulations for Hydrologic Network Design (SL 34–2013) [65] issued by the Ministry of Water Resources, the People's Republic of China. The densities and spatial distributions of all gauges meet the Technical Regulations for Hydrologic Network Design (SL 34-2013) [65] requirements.

Ground observations were conducted across the Tunxi Watershed with intense measurements within two representative 2nd-tier watersheds. There are three major types of general gauging stations across the Tunxi Watershed: rainfall gauging stations, comprehensive gauging stations that measure rainfall, soil moisture, and groundwater, and hydrological stations that measure streamflow and evaporation (Table 1). A network of nested hydrological stations serves as the fundamental gauging system for measuring streamflow and exploring the runoff concentration and propagation on multiple spatial scales. Within the 2nd-tier watersheds (Fig. 1(b)), more instruments are deployed, including integrated rainfall and soil moisture measurement systems, groundwater level monitoring platforms, flow weirs, array soil moisture gauging networks, rainfall gauging array, runoff component gauging systems, evaporation pan, meteorological station, lysimeter, and flux tower (Table 2 and Fig. 2). The rainfall and groundwater stations were roughly evenly distributed across the Tunxi Watershed and typical catchments. Soil moisture involving three spatial scales (Tunxi Watershed and 1st-tier and 2nd-tier watersheds) was also recorded. Three river discharge gauges are implemented in the Zhonghecun Watershed, Yuetan Watershed,

Table 1
Types and features of generic gauging stations implemented across the XAJ-NEW.

Gauging station type	Main features	Density of instruments ($set \cdot km^{-2}$)
Rainfall gauging station	Each station has one tipping bucket rain gauge that records rainfall every 5 min.	0.0075
Comprehensive gauging station	Each station has one tipping bucket rain gauge, four soil moisture sensors, and one groundwater (pressure water) level meter to measure rainfall, volumetric soil water content at depths of 10, 30, 40, and 60 cm, and groundwater level, respectively. Data are recorded every 5 min.	0.0037
Hydrological station	Each station has one flow level meter to measure water level and determine the corresponding flow discharge. Tunxi station has one evaporation pan to measure pan evaporation.	0.0011

Table 2
Types and features of instruments installed across the 2nd-tier watersheds within the XAJ-NEW.

Instruments	Main features	Density of instruments ($set \cdot km^{-2}$)	Image
Integrated rainfall and soil station	Each system has one tipping bucket rain gauge and four soil moisture sensors to measure rainfall and soil moisture at depths of 10, 30, 40, and 60 cm every 5 min.	20.69	Fig. 2(a)
Groundwater level station	Each station has one water level meter equipped with a data logger and solar panels to record groundwater depth every 5 min.	25.86	Fig. 2(b)
Flow weir	It is implemented in the rivulet channel and equipped with a laser level meter to automatically measure water level every 5 min.	6.90	Fig. 2(c)
Array soil moisture gauging network	There is an array of soil moisture stations in both 1st-Tier Watersheds I and II. 1st-Tier Watersheds I and II have 30 and 10 four-layer moisture-monitoring sites, respectively. Four sensors are inserted into the soil at the depths of 10, 30, 40, and 60 cm at each location. The data are recorded every 5 min.	1052.63	Fig. 2(d)
Rainfall gauging array	It measures rainfall interception by plant canopies with different densities. It comprises ten tipping bucket rain gauges evenly distributed within an area of 40 m^2. The data are recorded every 5 min.	1.72	Fig. 2(e)
Runoff component gauging system	A gauging system measures the runoff components in both 1st-tier Watersheds I and II. Each gauging station is equipped with four water weirs and five laser water level meters and measures surface runoff and interflows within three layers, i.e., 0–1, 1–2, and 2–3 m, every 5 min.	52.63	Fig. 2(f)
Evaporation pan	One evaporation pan observes the pan evaporation every 10 min.	1.72	Fig. 2(g)
Meteorological station	One meteorological station observes multiple meteorological elements every 10 min, including air temperature, relative humidity, wind speed, wind direction, precipitation, total radiation, soil moisture, and soil temperature.	1.72	Fig. 2(h)
Lysimeter	Two lysimeters measure soil evaporation, soil heat flux, soil moisture, soil temperature, electrical conductivity, and soil water potential at the depths of 10, 20, 40, 80, 120, and 180 cm. Data are recorded every 10 min.	1.72	Fig. 2(i)
Flux tower	The flux tower measures three-dimensional wind speeds and directions, water vapor, carbon dioxide, air	1.72	Fig. 2(j)

(continued on the next page)

Table 2 (*continued*)

Instruments	Main features	Density of instruments (set·km^{-2})	Image
	temperature, and light quantum at the height of 30 m, and soil heat flux at depths of 5, 10, and 15 cm. Gradient flux observation includes air temperature, relative humidity, and two-dimensional wind speed and direction at 25, 20, 15, 13, and 5 m. Other measured variables include four radiation components at 13 m, soil heat flux at a depth of 10 cm, and soil moisture at depths of 10, 40, and 100 cm.		

and Tunxi Watershed. In addition, several critical hydrological processes are observed within the typical catchments. The array rainfall station was instrumental in observing canopy rainfall interception. The runoff component gauging system observes the runoff components.

In summary, the instrument can observe hydrological processes, such as rainfall, soil water content, groundwater level, canopy interception, surface runoff, and interflow. The meteorological station and flux tower within the typical catchments also provide observations for meteorology, momentum, energy fluxes, and CO_2 fluxes. Observations in the XAJ-NEW, especially within the typical catchments, cover almost all important hydrological processes and key meteorological variables, providing a solid foundation for studying the hydrometeorological processes in this region, and mechanisms controlling these processes, and developing numerical methods to simulate these processes accurately. The data are automatically stored and transmitted through the wireless network. The reliability of the data was guaranteed through strict quality control software and manual post-processing and quality control. Moreover, the data and observation equipment are routinely checked and maintained.

3.3. Data analysis methods

3.3.1. Spatial interpolation

Based on the characteristics of hydrological variables, appropriate spatial interpolation methods are used to obtain the spatial distributions of hydrological variables from site-level observations. The CoKriging interpolation method was used to estimate the groundwater depth considering the relatively low station density and impact of terrain on the observed groundwater depth as follows [66,67]:

$$\begin{cases} \sum_{l=1}^{v}\sum_{i=1}^{nl}\lambda_{il}\gamma_{lv}(x_i,x_j)-\mu_v=\gamma_{uv}(x_j,x) \\ \sum_{i=1}^{nl}\lambda_{il}=\begin{cases}1, & 1=u\\ 0, & 0\neq u\end{cases}\end{cases} \tag{1}$$

$$\gamma_{uv}(h)=\frac{1}{2N(h)}\sum_{i=1}^{N(h)}[Z_u(x_i)-Z_u(x_i+h)][Z_v(x_i)-Z_v(x_i+h)] \tag{2}$$

where i and j are the origin and extremity number of the vector, n is the number of primary variables, l is the number of covariate variables, u and v are the primary (groundwater depth) and covariate (elevation) variables, respectively, λ is the weight associated with the data, γ is the value of the variogram, $Z(x)$ indicates the magnitude of the variable, and $N(h)$ is the total number of pairs of attributes that are separated by a distance h. Additionally, we applied the inverse distance weighting method to obtain the precipitation distribution in space.

3.3.2. Analysis of the spatial scaling effect of rainfall

The product moments (PM) method was used to assess the spatial scaling effect [68,69]. If a hydrological variable on one spatial scale can be transformed to another scale of equivalent distribution, it is considered scalable. Simple and multiscaling approaches are the two most common methods used to evaluate the scaling effects of hydrological variables [70,71]. If a hydrological process/-variable (X_i) at watershed i follows simple scaling, its moments and drainage area meet the following relationships:

$$\ln(E(X_i^k))=\ln(E(X_j^k))+b_k\ln(A_i) \tag{3}$$

$$b_k=\beta k \tag{4}$$

where $E\left(X_i^k\right)$ is the moment of order k for X_i, A_i is the drainage area, $E(X_j^k)$ is the moment of order k for X_j of the reference watershed, b_k is the fitted slope, and β is the scaling factor, which is a constant. The multiscaling approach is followed if the scaling factor is variable. Based on the observed rainfall data on multiple spatial scales, we evaluated the scaling effect of rainfall and assessed whether it met simple scaling.

3.3.3. Analysis of observed key water cycle components

We calculated the inter-site spatial correlation coefficients (R) of the soil water content at the four depths to investigate its spatial

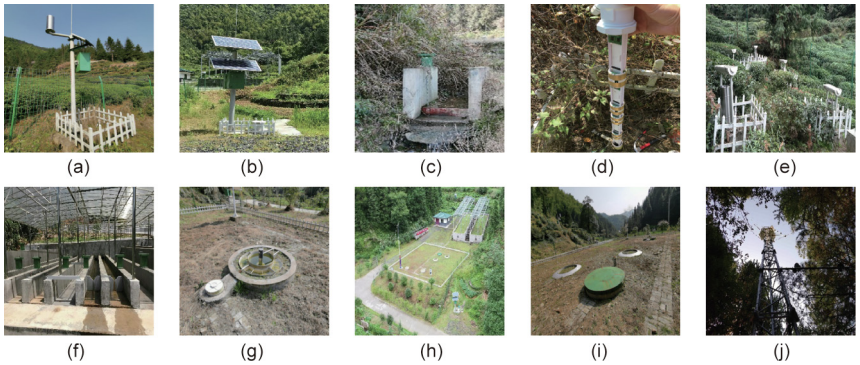

Fig. 2. Images of the instruments installed across the 2nd-tier watersheds: (a) integrated rainfall and soil moisture station, (b) groundwater level station, (c) flow weir, (d) array soil moisture gauging network, (e) rainfall gauging array, (f) runoff component gauging system, (g) evaporation pan, (h) meteorological station, (i) lysimeter, and (j) flux tower.

variability. The box–whisker plot, or box plot, represents the distribution of these correlation coefficients.

For canopy interception, we analyzed the statistical relationship between the canopy rainfall interception ratios (CRIR) measured by the array rainfall stations and the corresponding canopy leaf area index (LAI) measured using the LAI-2000 Plant Canopy Analyzer (Li-Cor, Inc., USA). Finally, we analyzed the observed runoff components at the 1st-tier Watershed I and compared the discharge processes across the XAJ-NEW on multiple spatial scales.

4. Preliminary results

4.1. Spatial scaling effect of rainfall

It is well known that rainfall exhibits great variability in space [72]. In this study, 30 rainfall stations, evenly distributed across the Tunxi Watershed (with a drainage area of 2674 km^2), were selected to identify the spatial scaling effects of rainfall. Correspondingly, 11 and 2 of the 30 rainfall stations are located within the Yuetan (drainage area of 854 km^2) and Zhonghecun watersheds (drainage area of 140 km^2), respectively. The PM method was used to examine the scaling effect of rainfall. The coefficient of variation (C_v) was used to evaluate the spatial variability of rainfall.

First, the linear relationship between $\ln(E(C_v))$ and $\ln(A)$ indicate that the drainage area reflects the main characteristics of the spatial variability of rainfall (Fig. 3(a)). Second, the fitted slope b_k (i.e., the slope of the$\ln(E(C_v^k)) \sim \ln(A)$ curve) is a linear function of k with the intercept close to zero (Fig. 3(b)), showing that the scaling factor of C_v is a constant (0.4258). The above results indicate C_v of rainfall across the Tunxi Watershed follows simple scaling and increases as the drainage area increases, leading to larger spatial heterogeneity.

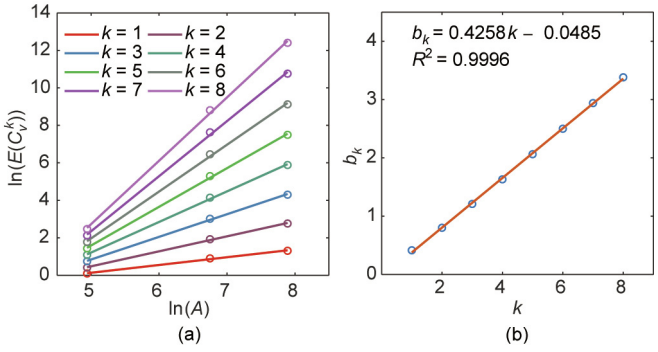

Fig. 3. Relationships (a) between the logarithm of mean value of coefficient of variation of the rainfall $\ln(E(C_v))$ and the logarithm of the watershed area ($\ln(A)$), and (b) between the fitted slope b_k and the moment of order k.

4.2. Rainfall and soil water content

The soil water content and rainfall were analyzed at two spatial scales: the Tunxi Watershed and typical catchments. The spatial-averaged soil water content of the Tunxi Watershed has a similar seasonality to that of the typical catchments (Fig. 4). The seasonal variations in the observed 5-min spatial-averaged soil water content in 2018 are shown in Figs. 4(a) and (b). The soil moisture of the top layer (10 cm) shows large variability and fluctuations between March and September for both the Tunxi Watershed and typical catchments (Fig. 4). The regional average soil water content shows an apparent vertical gradient, with soil moisture increasing with soil depth (Fig. 4), demonstrating the buffering effects of the soil column on the soil moisture. To investigate the spatial variability of soil water content, we also calculated the inter-site spatial correlation coefficients of the soil water content at depths of 10, 30, 40, and 60 cm (Figs. 4(c) and (d)). The mean inter-site correlation coefficient of the first layer (10 cm) is

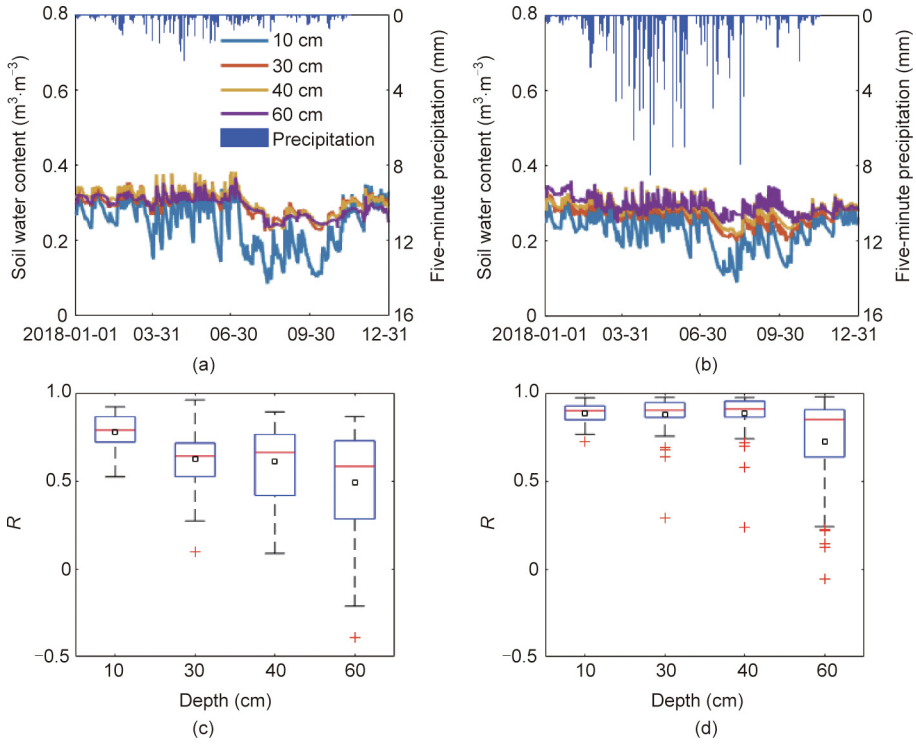

Fig. 4. Five-minute time series of site-averaged volumetric soil water content at four soil layers and rainfall in 2018 for (a) the 5th-tier Tunxi Watershed and (b) the 2nd-tier Watersheds I and II, and boxplots of inter-site correlation coefficients (R) at the four soil depths for (c) the 5th-tier Watershed Tunxi and (d) the 2nd-tier Watersheds I and II.

relatively high for the Tunxi Watershed, and typical catchments at 0.7758 and 0.8839, respectively, and decreases as soil depth increases, with the lowest values at the 60 cm layer (0.4882 and 0.7231) (Figs. 4(c) and (d)). Therefore, soil moisture has a higher spatial correlation on the surface and a lower spatial correlation underground. The mean inter-site correlation coefficient of the Tunxi Watershed at different depths ranges from 0.4882 to 0.7758 (Fig. 4(c)), while those of the typical catchments are above 0.7231 (Fig. 4(d)). These results demonstrate the distance-dependent correlation of soil moisture.

4.3. Groundwater depth

Groundwater depth was observed at the Tunxi Watershed and typical catchments. The temporal variations in the groundwater depth anomalies in 2018 are shown in Fig. 5. The groundwater level rises significantly from April to June and declines after July (Figs. 5(a) and (b)). The groundwater depth across the Tunxi Watershed ranges between −1.35 and 4.97 m relative to the 2018 yearly average (Fig. 5(a)), whereas the typical catchments have a much lower fluctuation, varying between −0.89 and 2.49 m (Fig. 5(b)). Tunxi Watershed has a larger elevation range and a much larger drainage area (1523 m and 2674 km^2, respectively) than the 2nd-tier typical watersheds (318 m and 0.58 km^2, respectively), contributing to the large spatial variability. In addition, the spatiotemporal distributions of precipitation, soil properties, and other geographical factors may also impact the variability of the groundwater level. We applied the CoKriging interpolation method [66] to estimate the spatial distribution of groundwater depth based on station observations. For the Tunxi Watershed, yearly average groundwater depth ranges from −7.64 to −0.07 m, with shallower water tables near the drainage network and downstream areas (Fig. 5(c)). Groundwater depths across the typical catchments have a much lower spatial variability (Fig. 5(d)) than the Tunxi Watershed because of the small area (only 0.58 km^2). In addition, the groundwater depths near the outlets and streams are lower (Fig. 5(d)). The ground surface elevation for the Tunxi Watershed and typical catchments is 96–1619 and 188–506 m, respectively. We conclude that topography variability and scale play an important role in controlling the spatial variability of groundwater depth across the Tunxi Watershed.

4.4. Canopy rainfall interception

Using the LAI-2000 Plant Canopy Analyzer, the canopy LAI over each rain bucket was measured on March 16, 2019. The LAI values over the nine rain buckets were 1.560, 1.150, 1.210, 0.388, 0.054, 0.000, 0.620, 0.010, and 0.301. Accordingly, we divided the samples into three categories: LAI ≥ 0.5, LAI < 0.5, and all LAI values. Rainfall above the canopy was selected as a reference to evaluate the interception function of the canopy. Twenty-nine rainfall events were used to analyze the relationship between CRIR and accumulated rainfall and LAI. CRIR decreases as the LAI decreases (Fig. 6). In addition, there is a logarithmic relationship between the interception ratio and accumulated rainfall (Fig. 6), consistent with the findings of Yu et al. [73]. As the accumulated rainfall increases, the CRIR decreases rapidly and gradually levels off (Fig. 6). In addition, LAI has a large impact on CRIR. Canopy with LAI ≥ 0.5 can intercept 20% of a rainfall totaling 51 mm, while canopy with LAI < 0.5 can only intercept 20% of a rainfall totaling 9 mm (Fig. 6). The relationship between CRIR, accumulated rainfall, and LAI can be used to estimate the canopy interception required in hydrological and ecological models [74,75].

4.5. Separation of runoff components

The gauging system can observe the surface runoff and interflow between 0–1, 1–2, and 2–3 m below ground in the XAJ-NEW. We chose a typical rainfall–runoff event of the 1st-tier Watershed I to analyze the surface runoff and interflow processes in 2018 (Fig. 7). Before this rainfall event (#2018042302), the typical catchments did not receive rainfall for several days, making

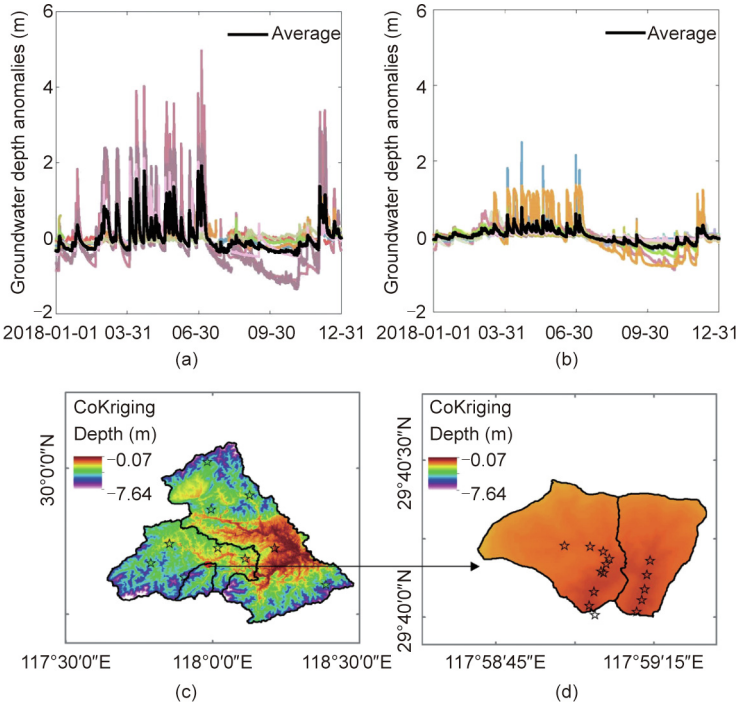

Fig. 5. Five-minute time series of site-wise (colored lines) and site-averaged (black lines) groundwater depth anomalies in 2018 for (a) the 5th-tier Tunxi Watershed and (b) the 2nd-tier Watersheds I and II, and spatial distributions of the 2018 yearly average groundwater depth across (c) the 5th-tier Tunxi Watershed and (d) the 2nd-tier Watersheds I and II interpolated by the CoKriging method; positive anomalies means shallow depth.

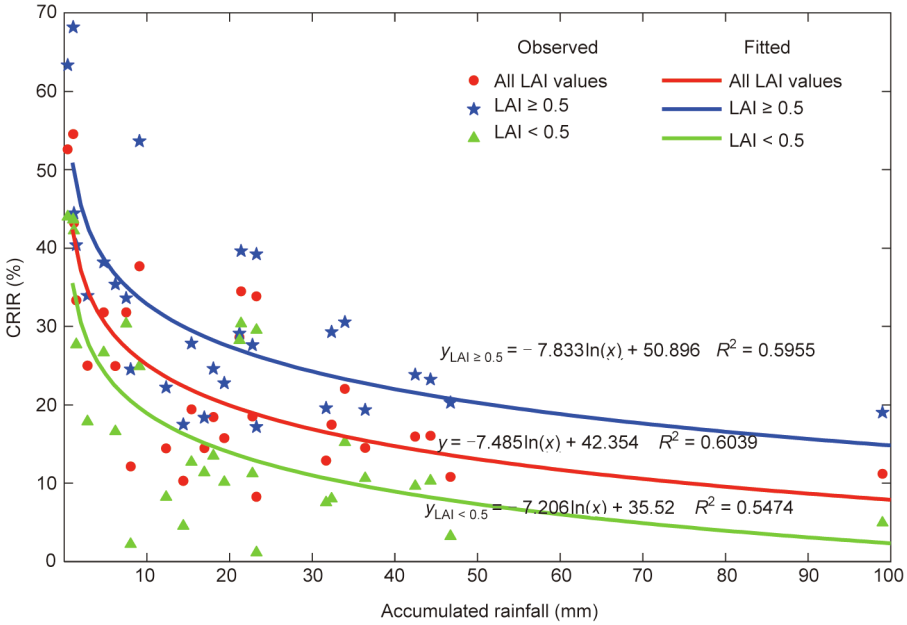

Fig. 6. Relationships between event-level canopy rainfall interception ratios (CRIR) and accumulated rainfall under different canopy densities (LAI). Point-level samples are grouped by their corresponding LAI categories (*i.e.*, LAI < 0.5, LAI ≥ 0.5, and all LAI values) and averaged to produce the data points.

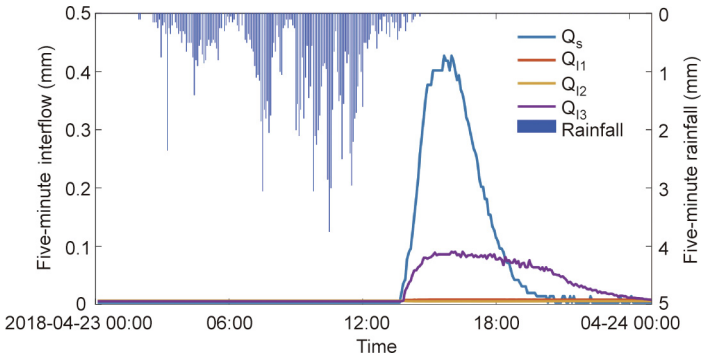

Fig. 7. Five-minute time series of observed four runoff components, namely, surface runoff (Q_s), and interflows of level 1 (0–1 m) (Q_{I1}), level 2 (1–2 m) (Q_{I2}), and level 3 (2–3 m) (Q_{I3}) at the outlet of the 1st-Tier Watershed I during the typical rainstorm event #2018042302.

the soil relatively dry and the mean soil water content at the 10 cm layer was 0.2 $m^3 \cdot m^{-3}$. Rainfall started at 2:10 AM on April 23, 2018. During the first 12 h, the rainwater infiltrated into the soil to fill the soil water deficit, and no runoff was generated (Fig. 7). As rainfall continued, runoffs start to yield and reach the peaks around 15:35 with surface runoff depth of 0.43 mm per 5 min and level 3 interflow depth (2–3 m) of 0.09 mm per 5 min around 15:55 (Fig. 7). For this event, the accumulated rainfall is 126.30 mm, while runoff depths for the surface, 0–1, 1–2, and 2–3 m layers, are 16.3 mm (12.9%), 2.24 mm (1.78%), 1.96 mm (1.55%), and 8.28 mm (6.55%), respectively. The 0–1 and 1–2 m layers yielded little interflow, suggesting that rainfall intensity may surpass the infiltration capacity during the peak period [76], and gravity plays an important role in interflow partitioning. In addition, surface runoff during this event shows a rapid rise and fast recession, while the interflow runoff in the 2–3 m layer is slower and flatter, indicating the regulation of the soil column on the hydrological processes.

4.6. Multiscale discharge

The discharge gauges were installed at the outlets of the Zhonghecun, Yuetan, and Tunxi Watersheds. As shown in Fig. 8, the hydrographs at the three discharge gauges show steep rising and falling limbs but with different durations. Tunxi has the longest flood, lasting (175.00 ± 73.61) h, followed by Yuetan ((160.33 ± 62.63) h) and Zhonghecun ((131.00 ± 36.89) h), indicating the influence of the size and water storage capacity of the watershed on flooding. Flood events #2019051220 and #2019052508 have narrow, steep, and single-peaked hydrographs at all three stations (Fig. 8). However, for flood event #2019061615, the hydrograph of Tunxi station has a double-peaked hydrograph corresponding to the double-peaked hyetograph, whereas the hydrographs of the Yuetan and Zhonghecun stations have a single-peak (Fig. 8). Because the Tunxi station is the outlet of the entire Tunxi Watershed and has a larger contributing area, more complex geographical characteristics and spatial variability of rainfall can produce a more complex hydrograph. Moreover, as a part of the Yuetan Watershed, the Zhonghecun station tends to reach flood peaks earlier than the Yuetan station (Fig. 8). However, the flood peak time at the Tunxi station is slightly shorter than that at the Yuetan station (Fig. 8). Furthermore, we produced a map of accumulated rainfall for each flood event using the inverse distance weighting method (Fig. 9). The first two events (#2019051220 and #2019052508) have relatively even rainfall across the region than the third event (#2019061615). The uneven temporal and spatial

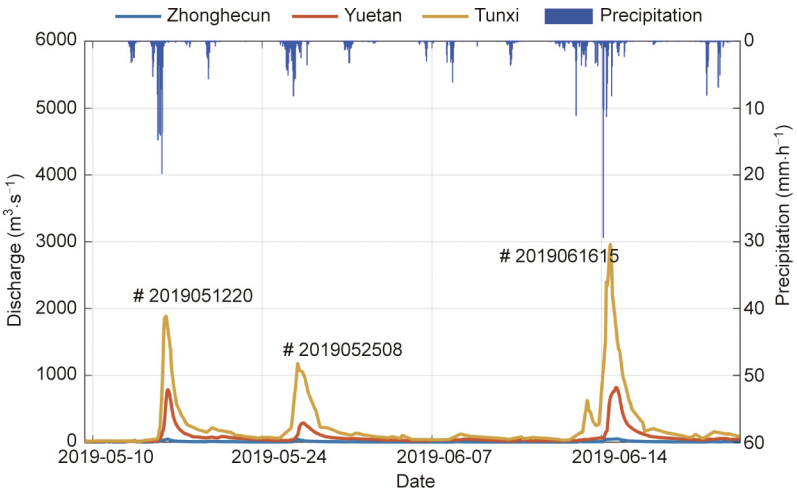

Fig. 8. Hourly time series of observed streamflow during the flood season of 2019 at the outlets of the 3rd-tier Zhonghecun Watershed, 4th-tier Yuetan Watershed, and 5th-tier Tunxi Watershed; there are three flood events (#2019051220, #2019052508, and #2019061615) during this period.

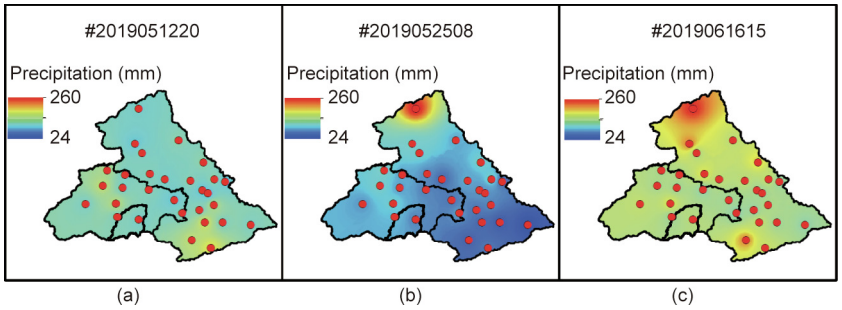

Fig. 9. Spatial distributions of observation-based accumulated rainfall during the three flood events in 2019: (a) Event #2019051220, (b) Event #2019052508, and (c) Event #2019061615.

distributions of rainfall (Fig. 8 and Fig. 9(c)) can explain the double-peaked hydrograph at Tunxi and the earlier flood peak occurrence at Yuetan than at Tunxi.

5. Summary

A spatially nested experimental watershed named XAJ-NEW was successfully built in the Xin'anjiang Watershed, making it the very first of its kind in the eastern China humid zone. Aimed at understanding the multiscale water cycle, this unique and comprehensive system can aid in observing a set of key hydrological elements and meteorological states. The system is designed for long-term operation and can provide more data in the future. The comprehensive experiment can quantify critical hydrological processes and reveal the underlying mechanisms controlling the hydrological and other relevant processes in the typical Chinese humid, hilly region. The existence and continuous operation of the XAJ-NEW system will be valuable to support systematic studies on the mechanisms of runoff generation and concentration, especially in the context of changing environments, and promote the development and improvement of hydrological, ecological, and land surface models. Further development of the XAJ-NEW system should focus on enhancing soil moisture observation across the whole root zone and implementing additional flux towers across this region to better monitor carbon and energy processes.

Acknowledgments

This work was supported by the National Natural Science Foundation of China (51879067), the National Key Research and Development Program of China (2016YFC0402701), the Fundamental Research Funds for the Central Universities of China (B200204038), the Natural Science Foundation of Jiangsu Province (BK20180022), and Six Talent Peaks Project in Jiangsu Province (NY-004). The observation data used in this study are available from http://hydro-lab.hhu.edu.cn.

Compliance with ethics guidelines

Ke Zhang, Yunping Li, Zhongbo Yu, Tao Yang, Junzeng Xu, Lijun Chao, Jin Ni, Liutong Wang, Yun Gao, Yuzhong Hu, and Zuoding Lin declare that they have no conflict of interest or financial conflicts to disclose.

References

[1] Lakshmi V. Use of satellite remote sensing in hydrological predictions in ungaged basins. In: Proceedings of 3rd International Conference on Education and Information Systems: Technologies and Applications; 2005 Jun 27–30; Hsinchu, China. New York City: IEEE; 2005. p. 85–9.
[2] Yu Z, Lakhtakia MN, Yarnal B, White RA, Miller DA, Frakes B, et al. Simulating the river-basin response to atmospheric forcing by linking a mesoscale meteorological model and hydrologic model system. J Hydrol 1999;218(1–2):72–91.

[3] Shi J, Zhao T, Du J, Ji D, Xiong C, Dong X, et al. Observing Earth's water cycle from space [Internet]. Bellingham: SPIE Newsroom; 2014 Nov 7 [cited 2021 Feb 18]. Available from: https://spie.org/news/5659-observing-earths-water-cycle-from-space?SSO=1.
[4] Murari RRV, Ruiz L, Sandhya C, Braun JJ, Mohan Kumar MS. Study of hydrological processes in a small forested watershed in South Karnataka (India). In: Venkatesh B, Purandara BK, Ramasastri S, editors. Forest Hydrology. National Seminar on Forest, Belgaum. New Delhi: Capital Publishing Company; 2007. p. 1–10.
[5] Talib A, Randhir TO. Climate change and land use impacts on hydrologic processes of watershed systems. J Water Clim Chang 2017;8(3):363–74.
[6] Beldring S, Engen-Skaugen T, Førland EJ, Roald LA. Climate change impacts on hydrological processes in Norway based on two methods for transferring regional climate model results to meteorological station sites. Tellus Ser A Dyn Meterol Oceanogr 2008;60(3):439–50.
[7] Ma X, Xu J, Luo Y, Prasad Aggarwal S, Li J. Response of hydrological processes to land-cover and climate changes in Kejie watershed, south–west China. Hydrol Processes 2009;23(8):1179–91.
[8] Yu Z, Pollard D, Cheng L. On continental-scale hydrologic simulations with a coupled hydrologic model. J Hydrol 2006;331(1–2):110–24.
[9] Zhang K, Kimball JS, Nemani RR, Running SW, Hong Y, Gourley JJ, et al. Vegetation greening and climate change promote multidecadal rises of global land evapotranspiration. Sci Rep 2015;5(1):15956.
[10] Trenberth KE, Asrar GR. Challenges and opportunities in water cycle research: WCRP contributions. Surv Geophys 2014;35(3):515–32.
[11] Coughlan M, Avissar R. The global energy and water cycle experiment (GEWEX) continental-scale international project (GCIP): an overview. J Geophys Res Atmos 1996;101(D3):7139–47.
[12] Chahine MT. GEWEX: the global energy and water cycle experiment. Eos 1992;73(2):9–14.
[13] Sorooshian S, Lawford R, Try P, Rossow W, Roads J, Polcher J, et al. Water and energy cycles: investigating the links. WMO Bull 2005;54(2):58–64.
[14] Nichols MH, Graaft JD, Cameron J, Sombatpanit S, Pieri C, Woodhill J. The Walnut Gulch Experimental Watershed—50 years of watershed monitoring and research. Enfiled: Science Publishers; 2007.
[15] Nichols MH, Renard K. History of the USDA-ARS Walnut Gulch Experimental Watershed. Reston: American Society of Civil Engineers; 2007. p. 107–12.
[16] Renard KG, Nichols MH, Woolhiser DA, Osborn HB. A brief background on the U.S. Department of Agriculture Agricultural Research Service Walnut Gulch Experimental Watershed. Water Resour Res 2008;44(5):W05S02.
[17] Yu Z, Fu X, Luo L, Lu H, Ju Q, Liu D, et al. One-dimensional soil temperature simulation with Common Land Model by assimilating *in situ* observations and MODIS LST with the ensemble particle filter. Water Resour Res 2014;50(8):6950–65.
[18] Šraj M, Rusjan S, Petan S, Vidmar A, Brilly M. The experimental watersheds in Slovenia. HNO 2008;4(1):012051.
[19] Blume T, Van Meerveld I, Weiler M. The role of experimental work in hydrological sciences—insights from a community survey. Hydrol Sci J 2017;62(3):334–7.
[20] Hopmans J, Pasternack G. Experimental hydrology: a bright future. Adv Water Resour 2006;29(2):117–20.
[21] Minea G, Rodrigo-Comino J, Moroșanu G. Playing with water—an introduction to experimental hydrology. Forum Geografic 2018;XVII:56–65.
[22] Kirkby M. Hillslope runoff processes and models. J Hydrol 1988;100(1–3):315–39.
[23] Bronstert A. Capabilities and limitations of detailed hillslope hydrological modelling. Hydrol Processes 1999;13(1):21–48.
[24] Shahedi K. Hillslope hydrological modeling: the role of bedrock geometry and hillslope–stream interaction. Wageningen: Wageningen University; 2008.
[25] Clark MP, Rupp DE, Woods RA, Tromp-van Meerveld HJ, Peters NE, Freer JE. Consistency between hydrological models and field observations: linking processes at the hillslope scale to hydrological responses at the watershed scale. Hydrol Processes 2009;23(2):311–9.
[26] Hankin B, Metcalfe P, Beven K, Chappell NA. Integration of hillslope hydrology and 2D hydraulic modelling for natural flood management. Hydrol Res 2019;50(6):1535–48.
[27] Zhao RJ. Watershed hydrological model—Xinanjiang Model and Shanbei Model. Beijing: Water Resource and Electric Press; 1984.
[28] Hewlett JD, Troendle CA. Non-point and diffused water sources: a variable source area problem. In: Proceedings of Symposium on Watershed Management by ASCE Irrigation and Drainage Division; 1975 Aug 11–13, Logan, UT, USA. New York City: American Society of Civil Engineers; 1975. p. 21–46.
[29] Dunne T, Black RD. Partial area contributions to storm runoff in a small New England Watershed. Water Resour Res 1970;6(5):1296–311.
[30] Hewlett JD. Soil moisture as a source of baseflow from steep mountain watersheds. Report. Asheville: US Department of Agriculture, Forest Service, Southeastern Forest Experimental Station; 1961.
[31] Bergström S, Lindström G. Interpretation of runoff processes in hydrological modelling—experience from the HBV approach. Hydrol Processes 2015;29(16):3535–45.
[32] Bergström S, Forsman A. Development of a conceptual deterministic rainfall—runoff model. Nord Hydrol 1973;4(3):240–53.
[33] Kirkby MJ. Hillslope hydrology. New York City: Chichester: Wiley; 1978.
[34] Liang X, Lettenmaier DP, Wood E, Burges SJ. A simple hydrologically based model of land surface water and energy fluxes for general circulation models. J Geophys Res Atmos 1994;99(D7):14415–28.
[35] Li ZJ, Zhang K. Comparison of three GIS-based hydrological models. J Hydrol Eng 2008;13(5):364–70.
[36] Savenije HH. HESS opinions "topography driven conceptual modelling (FLEX-Topo)". Hydrol Earth Syst Sci 2010;14(12):2681–92.
[37] Gao H, Hrachowitz M, Fenicia F, Gharari S, Savenije H. Testing the realism of a topography-driven model (FLEX-Topo) in the nested catchments of the Upper Heihe. China Hydrol Earth Syst Sci 2014;18(5):1895–915.
[38] Gao H, Birkel C, Hrachowitz M, Tetzlaff D, Soulsby C, Savenije HH. A simple topography-driven and calibration-free runoff generation module. Hydrol Earth Syst Sci 2019;23(2):787–809.
[39] Liu Y, Zhang K, Li Z, Liu Z, Wang J, Huang P. A hybrid runoff generation modelling framework based on spatial combination of three runoff generation schemes for semi-humid and semi-arid watersheds. J Hydrol 2020;590:125440.
[40] Li X, Cheng G, Liu S, Xiao Q, Ma M, Jin R, et al. Heihe Watershed Allied Telemetry Experimental Research (HiWATER): scientific objectives and experimental design. Bull Am Meteorol Soc 2013;94(8):1145–60.
[41] Yang K, Qin J, Zhao L, Chen Y, Tang W, Han M, et al. A multiscale soil moisture and freeze–thaw monitoring network on the third pole. Bull Am Meteorol Soc 2013;94(12):1907–16.
[42] Zhao P, Xu X, Chen F, Guo X, Zheng X, Liu L, et al. The third atmospheric scientific experiment for understanding the Earth–Atmosphere coupled system over the Tibetan Plateau and its effects. Bull Am Meteorol Soc 2018;99(4):757–76.
[43] Levang SJ, Schmitt RW. Centennial changes of the global water cycle in CMIP5 models. J Clim 2015;28(16):6489–502.
[44] Huntington TG. Evidence for intensification of the global water cycle: review and synthesis. J Hydrol 2006;319(1–4):83–95.
[45] Forzieri G, Miralles DG, Ciais P, Alkama R, Ryu Y, Duveiller G, et al. Increased control of vegetation on global terrestrial energy fluxes. Nat Clim Chang 2020;10(4):356–62.
[46] Davies EGR, Simonovic SP. Climate change and the hydrological cycle. In: Proceedings of 17th Canadian Hydrotechnical Conference. Hydrotechnical Engineering: Cornerstone of a Sustainable Environment; 2005 Aug 17–19; Edmonton, AB, Canada. Surrey: Canadian Society for Civil Engineering; 2005. p. 47–58.
[47] Osborn TJ, Gosling SN, Wallace CJ, Dorling S. The water cycle in a changing climate. In: Proceedings of 7th World Water Forum, Words Into Action; 2015 Apr 13; Dargu: Republic of Korea. Marseille: World Water Council; 2015. p.14–9.
[48] Tang Q, Durand M, Lettenmaier DP, Hong Y. Satellite-based observations of hydrological processes. Int J Remote Sens 2010;31(14):3661–7.
[49] Troch PA, Dijksma R, van Lanen HAJ; van Loon E. Towards improved observations and modeling of catchment-scale hydrological processes: bridging the gap between local knowledge and the global problem of ungauged catchments. In: Proceedings of Workshop of the IAHS Decade on Prediction in Ungaged Basins, Brazil; 2002 Nov 20–22; Brasilia: University of Brasilia; 2002. p. 395–403.
[50] Liu J, Chen X, Zhang X, Hoagland K. Grid digital elevation model based algorithms for determination of hillslope width functions through flow distance transforms. Water Resour Res 2012;48(4):W04532.
[51] Sivapalan M. Process complexity at hillslope scale, process simplicity at the watershed scale: is there a connection? Hydrol Processes 2003;17(5):1037–41.
[52] Yu Z, Carlson TN, Barron EJ, Schwartz FW. On evaluating the spatial–temporal variation of soil moisture in the Susquehanna River Basin. Water Resour Res 2001;37(5):1313–26.
[53] Zhao R. The Xinanjiang Model applied in China. J Hydrol 1992;135(1–4):371–81.
[54] Wu C, Huang G, Yu H, Chen Z, Ma J. Impact of climate change on reservoir flood control in the upstream area of the Beijiang River Basin, South China. J Hydrometeorol 2014;15(6):2203–18.
[55] Xu Y, Huang X, Zhang Y, Lin W, Lin E. Statistical analyses of climate change scenarios over China in the 21st century. Adv Clim Chang Res 2006;2(Supp 1):50–3.
[56] Fu G, Yu J, Yu X, Ouyang R, Zhang Y, Wang P, et al. Temporal variation of extreme rainfall events in China, 1961–2009. J Hydrol 2013;487(487):48–59.
[57] Qin N, Chen X, Fu G, Zhai J, Xue X. Precipitation and temperature trends for the Southwest China: 1960–2007. Hydrol Processes 2010;24(25):3733–44.
[58] Zhou R, Li Y, Lu D, Liu H, Zhou H. An optimization based sampling approach for multiple metrics uncertainty analysis using generalized likelihood uncertainty estimation. J Hydrol 2016;540:274–86.
[59] Lin K, Lian Y, He Y. Effect of baseflow separation on uncertainty of hydrological modeling in the Xinanjiang Model. Math Probl Eng 2014;2014:985054.
[60] Ju Q, Yu Z, Hao Z, Ou G, Zhao J, Liu D. Division-based rainfall–runoff simulations with BP neural networks and Xinanjiang Model. Neurocomputing 2009;72(13–15):2873–83.
[61] Mao G, Liu J. WAYS v1: a hydrological model for root zone water storage simulation on a global scale. Geosci Model Dev 2019;12(12):5267–89.
[62] Li Z, Liu M, Zhao Y, Liang T, Sha J, Wang Y. Application of regional nutrient management model in Tunxi Catchment: in support of the trans-boundary eco-compensation in eastern China. Clean 2014;42(12):1729–39.

[63] Qi Z, Kang G, Chu C, Qiu Y, Xu Z, Wang Y. Comparison of SWAT and GWLF model simulation performance in humid South and semi-arid North of China. Water 2017;9(8):567.
[64] Zhao J, Xu J, Cheng L, Jin J, Li X, Chen N, et al. The evolvement mechanism of hydro-meteorological elements under climate change and the interaction impacts in Xin'anjiang Basin, China. Stochastic Environ Res Risk Assess 2019;33(4–6):1159–73.
[65] Ministry of Water Resources of the People's Republic of China. SL 34–2013: technical regulations for hydrologic network design. Chinese standard. Beijing: Ministry of Water Resources of the People's Republic of China; 2013.
[66] Hoeksema RJ, Clapp RB, Thomas AL, Hunley AE, Farrow ND, Dearstone KC. Cokriging model for estimation of water table elevation. Water Resour Res 1989;25(3):429–38.
[67] Ahmadi SH, Sedghamiz A. Application and evaluation of kriging and CoKriging methods on groundwater depth mapping. Environ Monit Assess 2008;138(1–3):357–68.
[68] Smith JA. Representation of basin scale in flood peak distributions. Water Resour Res 1992;28(11):2993–9.
[69] Kumar P, Guttarp P, Foufoula-Georgiou E. A probability-weighted moment test to assess simple scaling. Stoch Hydrol Hydraul 1994;8(3):173–83.
[70] Basu B, Srinivas VV. A recursive multi-scaling approach to regional flood frequency analysis. J Hydrol 2015;529:373–83.
[71] Skaugen T, Vaeringstad T. A methodology for regional flood frequency estimation based on scaling properties. Hydrol Processes 2005;19(7):1481–95.
[72] Mandapaka PV, Krajewski WF, Mantilla R, Gupta VK. Dissecting the effect of rainfall variability on the statistical structure of peak flows. Adv Water Resour 2009;32(10):1508–25.
[73] Yu Y, Gao T, Zhu J, Wei X, Guo Q, Su Y, et al. Terrestrial laser scanning-derived canopy interception index for predicting rainfall interception. Ecohydrology 2020;12(5):e2212.
[74] Zheng C, Jia L. Global canopy rainfall interception loss derived from satellite earth observations. Ecohydrology 2020;13(2):e2187.
[75] Miralles DG, Gash JH, Holmes TRH, de Jeu RAM, Dolman AJ. Global canopy interception from satellite observations. J Geophys Res Atmos 2010;115(D16):D16122.
[76] Horton RE. The Rôle of infiltration in the hydrologic cycle. Eos 1933;14(1):446–60.